

**ADVANCING PATHOGEN DIAGNOSTICS USING
SURFACE ENHANCED RAMAN SPECTROSCOPY
(SERS) WITH GLANCING ANGLE DEPOSITION
FABRICATED SUBSTRATES FOR MICROBIAL
DETECTION**

Sneha Senapati



SCHOOL OF INTERDISCIPLINARY RESEARCH (SIRe)

INDIAN INSTITUTE OF TECHNOLOGY DELHI

SEPTEMBER 2025

©Indian Institute of Technology Delhi (IITD), New Delhi, 2025

**ADVANCING PATHOGEN DIAGNOSTICS USING
SURFACE ENHANCED RAMAN SPECTROSCOPY
(SERS) WITH GLANCING ANGLE DEPOSITION
FABRICATED SUBSTRATES FOR MICROBIAL
DETECTION**

by

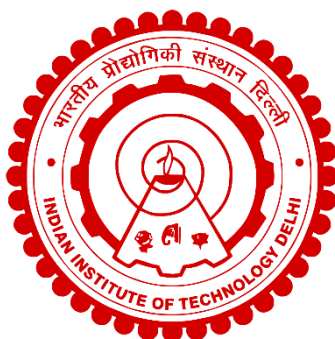
Sneha Senapati

School of Interdisciplinary Research (SIRe)

Submitted

*in fulfilment of requirements of degree of Doctor of
Philosophy*

to the



INDIAN INSTITUTE OF TECHNOLOGY DELHI

September 2025

Dedication

This dissertation is dedicated to my parents, ***Mr. Pitabash Senapati*** and ***Mrs. Pushpa Senapati***. It is their blessings, encouragement, and constant love that has brought me here. Their support and understanding have sustained me throughout my life. I will never be able to repay the blessings and sacrifices they have bestowed upon me. The living GOD of my life.

CERTIFICATE

I am satisfied that the thesis entitled “**ADVANCING PATHOGEN DIAGNOSTICS USING SURFACE ENHANCED RAMAN SPECTROSCOPY (SERS) WITH GLANCING ANGLE DEPOSITION FABRICATED SUBSTRATES FOR MICROBIAL DETECTION**” submitted by Ms. Sneha Senapati is worthy of consideration for the award of the degree of **Doctor of Philosophy** and is a record of original and bonafide research work carried out by him under our supervision. The results contained in it have not been submitted in part or full to any other university or institute for the award of any degree/diploma.

Prof. J.P. Singh

Department of Physics
Indian Institute of Technology Delhi
New Delhi-110016, India

Dr. Smita S. Kulkarni

Former Emeritus Scientist
Former Head & Scientist G
Indian Council of Medical Research
New Delhi-110029, India

Date: 8th September 2025

ACKNOWLEDGEMENTS

The journey of this doctoral thesis might have been a fond illusion without the contribution and support from many inspiring individuals that create a productive environment for me to work in. Therefore, I would like to express my sincere gratitude to all the people who contributed to forming such a stimulating atmosphere that helped me over the years to complete my work successfully.

*Firstly, I wish to acknowledge my sincere gratitude towards my thesis supervisor **Prof. J.P. Singh and Dr. Smita S. Kulkarni**, who contributed significantly to shaping and guiding the direction for my thesis work. I am profoundly grateful to both for providing me with an environment where I learned from their knowledge, experience and wisdom that enabled me to complete this study. They have always inspired me with his endless patience, in-depth knowledge, and dedication to accomplish tasks at stipulated time. The allegiance with which they handle such a large group and are always willing to give new ideas and implement them is highly motivational. They have been my guiding stars for both professional and personal life. I am lucky to have them both as my supervisors.*

*Besides my supervisors, I sincerely thank and appreciate the efforts of the SRC members, **Prof. Neeraj Kare, Prof. Sunil Kumar, and Prof. Anuj Dhawan**, for their ever-helping approach and supportive nature.*

I am thankful to **Prof. Rajendra Singh, Prof. Hemant K Kashyap, Prof. Nilanjan Senroy, and Prof. B. Premachandran** Head of the Department, School of Interdisciplinary Research, IIT Delhi, for providing necessary facilities.

I express my deep gratitude towards **Prof. Neetu Singh** (Center for Biomedical Engineering, IIT Delhi), **Dr. Vidya Arankalle** (Interactive Research School for Health Affairs (IRSHA), Pune), **Dr. Rashmi Virkar** (IRSHA, Pune), **Prof. Ishaan Gupta** (Centre for Biochemical Engineering and Biotechnology, IIT Delhi), **Dr. B.R. Mirdha** (Professor of Microbiology, All India Institute for Medical Sciences (AIIMS) Delhi) for providing their guidance and support throughout my Ph.D. journey.

I also thank **Dr. Pradeep Singh** (NRF, IIT Delhi) and **Dr. Sakshi Kapoor** (NRF, IIT Delhi), who performed many experiments along with me and provided valuable suggestions on writing and understanding many aspects of research. I must not forget **Dr. Yogita Maithani**, who has constantly been my guiding light throughout my journey. An always go-to senior and friend who holds a special place in my heart. I gratefully acknowledge the **Nanoscale Research Facility (NRF)** and **Central Research Facility (CRF)** at the Indian Institute of Technology Delhi for providing experimental facilities during this course of work.

I feel fortunate to be associated with **GLAD and Nano-CVD Lab**, which brings along an immense history of research and a tradition of dedication and innovation. I would also like to thank my seniors **Dr. Sarjana Yadav, Dr. Jyoti Yadav, Dr. Jamal Ahmad Khan, Dr. Arvind Kaushik** and my lab mates, **Dr. Siddharth Rana, Shivam Singh, C.M. Vidhya, Lakshay Bharadwaj, Debottam Dutta,**

Simranjeet Kaur, Deepali, Vandana and Priyanka for their encouragement and scientific discussions. I wish to extend my thanks and regards **Mrs. Jyoti Choudhury** who has always been helping hand in technical and non-technical aspects of research. Also, without her as a very special friend and well-wisher this journey would have been impossible. I am obliged to be associated with such a large group and helping colleagues at GLAD and Nano-CVD Lab.

My special thanks to my collaborators **Dr. Manleen Kaur, Mr. Rajan and Mr. Aditya Singh** for their endeavoring support and help throughout the PhD journey.

I wish to extend heartfelt thanks to **Dr. Arvind Kaushik** for being by my side during the peak times and being a great collaborator and friend. Also, my special thanks to my friend at IIT Delhi **Dr. Siddharth, Mr. Sandeep and Ms. Akshi**. And my very special and lovely roommates **Mrs. Anshika, Ms. Tamkeen, Ms. Hirah, Ms. Anam**, for their constant presence. I am deeply grateful to my everlasting, low maintenance friends **Ms. Nikita Nanaware, Dr. Pallavi, Dr. Monalisa, and my school friends** for their constant love, laughter, and unwavering support throughout this journey. Their friendship and support were a great source of encouragement and have spent the most enlightening time of my research life. I sincerely thank and acknowledge the useful comments and insightful discussions that have helped me throughout my doctorate journey.

I am delighted to express my sincere appreciation to **my family** for their love, support and understanding that allowed me to nurture my dream and keep looking forward to more exceptional achievements in the future. I am incredibly grateful to

Babu and **Maa** and my siblings, **Dr. Sriya and Mr. Subham**, who encouraged and helped me at every stage of my personal and academic life and longed to see this achievement come true.

I gratefully acknowledge the IIT Delhi for providing funding support and Senior Research Fellowship for this study.

Above all, I owe it all to Almighty God and **my late grandparents** for immense blessings and granting me the wisdom, health, and strength to complete this task and enabling me to compile it.

Sneha Senapati

Date: 08-09-2025

Place: New Delhi

ABSTRACT

The relentless rise of infectious diseases, the global threat of antimicrobial resistance (AMR), and the continuous emergence of viral variants have created an urgent demand for rapid, ultrasensitive, and cost-effective diagnostic technologies. Traditional diagnostic tools, while effective, often fall short in sensitivity, speed, and adaptability, especially in resource-limited settings. In this context, Surface-Enhanced Raman Scattering (SERS) has emerged as a transformative analytical technique, capable of detecting molecular signatures at ultralow concentrations with high specificity and rapid turnaround times. This thesis presents a comprehensive development of next-generation SERS-based platforms by combining advanced nanofabrication, innovative substrate engineering, and cutting-edge machine learning algorithms. These platforms target the detection and differentiation of bacterial, viral, and parasitic pathogens, offering powerful solutions that bridge the critical gap between laboratory research and real-world clinical applications.

Firstly, we present the fabrication of a novel paper-based SERS substrate by integrating zigzag silver nanorods (AgNRs) onto simple office paper via the glancing angle deposition (GLAD) method. The porous and fibrous architecture of the paper provides an intrinsically high surface area and roughness, which, combined with the unique two-armed zigzag morphology of AgNRs, generates dense plasmonic hotspots, amplifying Raman signals significantly. This cellulose-AgNR hybrid substrate offers critical advantages, including flexibility,

biodegradability, and low manufacturing costs, addressing key limitations of conventional rigid substrates. Application of the platform to the detection of nosocomial infection-causing bacteria — *Pseudomonas aeruginosa*, *Escherichia coli*, and *Staphylococcus aureus* — demonstrated an impressive limit of detection (LOD) of 10^2 copies/mL. Notably, the SERS intensity recorded on the paper-based substrate was approximately ten-fold higher than that observed on conventional glass-based substrates. Furthermore, a clear spectral differentiation between Gram-positive and Gram-negative bacteria was achieved, highlighting the platform’s diagnostic potential for broad-spectrum bacterial identification.

Building on this foundation, we expanded the utility of AgNR-based SERS platforms toward viral detection, focusing specifically on the differentiation of SARS-CoV-2 variants and co-variants. Pristine AgNR substrates fabricated via GLAD were employed for the sensitive detection and strain-level differentiation of clinically relevant variants, including Wild type, Kappa, Delta, and Omicron strains, and Omicron sub-variants BA.1, BA.2, BA.5, and XBB. However, the highly similar genetic and biochemical profiles of these variants posed significant challenges for traditional SERS analysis. To overcome this, machine learning (ML) algorithms were integrated with SERS data to extract subtle spectral variations beyond human discernment. Support Vector Machine (SVM) and Bidirectional Long Short-Term Memory (BiLSTM) models were trained on SERS spectra obtained from 122 positive nasopharyngeal swab (NPS) samples, previously confirmed by next-generation sequencing (NGS). The SVM classifier

achieved a variant classification accuracy of 89% on the validation set, outperforming the BiLSTM model, which achieved 86%. When tested on an independent blind set, SVM and BiLSTM achieved accuracy of 75% and 70.09%, respectively. Moreover, for subvariants classification among Omicron strain, the SVM model achieved a remarkable 96% accuracy. These results demonstrate that coupling SERS with ML substantially enhances the resolution and precision of variant detection, offering a promising pathway for real-time epidemiological surveillance.

In parallel, recognizing the importance of rapid antimicrobial susceptibility testing (AST), we developed a novel bimetallic SERS substrate composed of gold nanoislands decorated onto silver nanorods (AuNI@AgNR), again fabricated using GLAD and thermal deposition. The addition of gold nanoislands not only enhanced the stability of the substrate against oxidation but also significantly improved plasmonic coupling, resulting in greater electromagnetic field enhancement. The AuNI@AgNR substrate enabled the detection of bacterial pathogens at ultra-low concentrations down to 1 CFU/mL, both in single and mixed bacterial cultures. The platform effectively distinguished between Gram-positive and Gram-negative bacteria and was used to determine the minimum inhibitory concentrations (MICs) for various bacterial strains in a rapid manner. Partial least squares discriminant analysis (PLS-DA) further allowed clear classification between antibiotic-susceptible and resistant strains, underscoring the substrate's utility for rapid AMR profiling. Importantly, the ability to differentiate and monitor bacterial populations in polymicrobial infections

represents a major advancement toward real-world, point-of-care (POC) applications.

Lastly, to address the burden of parasitic infections, a portable SERS platform was developed for malaria detection in blood samples, exploiting the paramagnetic properties of hemozoin — a crystalline byproduct unique to the malaria parasite. Using AgNR substrates fabricated via GLAD, an external magnetic field of 0.3 T was applied during Raman measurements, resulting in a remarkable tenfold enhancement of the SERS signal intensity compared to non-magnetized measurements. This magnetic assistance allowed an unprecedented LOD of 10^{-14} M (approximately 6 parasites/ μ L), vastly surpassing conventional detection limits. Through systematic dilution studies, it was demonstrated that hemozoin signals dominated the SERS spectra as hemoglobin-associated peaks diminished, validating the preferential localization of hemozoin at electromagnetic hotspots under magnetic influence. Principal component analysis (PCA) of SERS spectra from healthy and malaria-positive whole blood and plasma samples revealed distinct clustering, demonstrating the reliability and robustness of this method. Notably, magnetized and non-magnetized malaria-positive samples occupied separate regions in PCA space, highlighting the significant impact of magnetic field enhancement on detection fidelity.

Overall, this thesis demonstrates the immense potential of integrating advanced nanomaterials, SERS techniques, and machine learning algorithms to establish powerful, flexible, and sensitive platforms for the detection of bacterial, viral, and

parasitic pathogens. The developed strategies not only push the boundaries of sensitivity and specificity but also pave the way toward real-world applications in clinical diagnostics, epidemic surveillance, and antimicrobial stewardship. Future directions of this work involve the translation of these platforms into fully integrated portable devices, further improving accessibility, affordability, and applicability in resource-limited settings.

सार

संक्रामक रोगों की निरंतर बढ़ती घटनाएँ, एंटीमाइक्रोबियल रेज़िस्टेंस (AMR) का वैश्विक खतरा, और लगातार उभरते नए वायरल वेरिएंट्स ने तीव्र, अति-संवेदनशील तथा किफ़ायती डायग्नोस्टिक तकनीकों की तत्काल आवश्यकता उत्पन्न कर दी है। पारंपरिक डायग्नोस्टिक उपकरण, यद्यपि प्रभावी हैं, परंतु संवेदनशीलता, गति और अनुकूलनशीलता के मामले में अक्सर कमतर सिद्ध होते हैं, विशेष रूप से संसाधन-सीमित परिस्थितियों में। इस परिप्रेक्ष्य में, सरफेस-एन्हांस्ड रमन स्कैटरिंग (SERS) एक परिवर्तनकारी विश्लेषणात्मक तकनीक के रूप में उभरी है, जो अत्यंत निम्न सांद्रता पर भी आणविक संकेतों का उच्च विशिष्टता और तीव्र परिणाम समय के साथ पता लगाने में सक्षम है। प्रस्तुत शोध प्रबंध में, उन्नत नैनोफैब्रिकेशन, अभिनव सबस्ट्रेट इंजीनियरिंग और अत्याधुनिक मशीन लर्निंग एल्गोरिद्म को संयोजित करते हुए अगली पीढ़ी के SERS-आधारित प्लेटफॉर्म के व्यापक विकास को प्रस्तुत किया गया है। ये प्लेटफॉर्म बैक्टीरियल, वायरल और परजीवी रोगजनकों की पहचान और विभेदन को लक्षित करते हैं, तथा प्रयोगशाला अनुसंधान और वास्तविक नैदानिक अनुप्रयोगों के बीच की महत्वपूर्ण खाई को पाटने हेतु सक्षम समाधान प्रदान करते हैं।

प्रथम चरण में, हमने एक अभिनव पेपर-आधारित SERS सबस्ट्रेट का निर्माण प्रस्तुत किया है, जिसमें ग्लैसिंग एंगल डिपोज़िशन (GLAD) पद्धति द्वारा साधारण ऑफिस पेपर पर ज़िगज़ैग सिल्वर नैनोरॉड्स (AgNRs) को एकीकृत किया गया। पेपर की छिद्रपूर्ण और तंतुयुक्त संरचना उच्च सतही क्षेत्र और खुरदरापन प्रदान करती है, जो AgNRs की द्विशाखीय ज़िगज़ैग आकृति के साथ मिलकर सघन प्लाज़्मोनिक हॉटस्पॉट्स उत्पन्न करती है, जिससे रमन संकेतों का तीव्र प्रवर्धन होता है। यह सेल्यूलोज़-AgNR हाइब्रिड सबस्ट्रेट लचीलापन, बायोडिग्रेडेबिलिटी और कम निर्माण लागत जैसी महत्वपूर्ण

विशेषताएँ प्रदान करता है, जो पारंपरिक कठोर सबस्ट्रेट्स की सीमाओं को दूर करता है। इस प्लेटफॉर्म को अस्पताल-संबंधी संक्रमण उत्पन्न करने वाले बैक्टीरिया — *Pseudomonas aeruginosa*, *Escherichia coli*, और *Staphylococcus aureus* — की पहचान हेतु प्रयोग में लाया गया, जहाँ प्रभावशाली 10^2 copies/mL की लिमिट ऑफ डिटेक्शन (LOD) प्राप्त हुई। उल्लेखनीय रूप से, पेपर-आधारित सबस्ट्रेट पर दर्ज SERS तीव्रता पारंपरिक ग्लास-आधारित सबस्ट्रेट की तुलना में लगभग दस गुना अधिक थी। इसके अतिरिक्त, ग्राम-पॉज़िटिव और ग्राम-नेगेटिव बैक्टीरिया के बीच स्पष्ट स्पेक्ट्रल विभेदन प्राप्त हुआ, जिससे प्लेटफॉर्म की व्यापक डायग्नोस्टिक क्षमता उजागर होती है।

इसके आधार पर, हमने AgNR-आधारित SERS प्लेटफॉर्म की उपयोगिता को वायरल पहचान की दिशा में विस्तारित किया, विशेष रूप से SARS-CoV-2 वेरिएंट्स और सह-वेरिएंट्स के विभेदन पर केंद्रित होकर। GLAD द्वारा निर्मित शुद्ध AgNR सबस्ट्रेट्स का उपयोग *Wild type*, *Kappa*, *Delta*, *Omicron* स्ट्रेन्स तथा *Omicron BA.1*, *BA.2*, *BA.5*, और *XBB* सबवेरिएंट्स की संवेदनशील पहचान और स्ट्रेन-स्तरीय विभेदन के लिए किया गया। हालाँकि, इन वेरिएंट्स की अत्यधिक समान आनुवंशिक और बायोकेमिकल प्रोफ़ाइल ने पारंपरिक SERS विश्लेषण के लिए गंभीर चुनौतियाँ प्रस्तुत कीं। इसे पार करने हेतु, मशीन लर्निंग (ML) एल्गोरिद्म को SERS डेटा के साथ एकीकृत किया गया ताकि मानव विवेचना से परे सूक्ष्म स्पेक्ट्रल भिन्नताओं को निकाला जा सके। सपोर्ट वेक्टर मशीन (SVM) और बिडायरेक्शनल लॉन्ग शॉर्ट-टर्म मेमोरी (BiLSTM) मॉडलों को 122 पॉज़िटिव नेज़ोफैरिन्जियल स्वैब (NPS) नमूनों से प्राप्त SERS स्पेक्ट्रा पर प्रशिक्षित किया गया, जिनकी पूर्व पुष्टि नेक्स्ट-जनरेशन सीक्वेंसिंग (NGS) द्वारा की गई थी। वेलिडेशन सेट पर SVM क्लासिफ़ायर ने 89% की वर्गीकरण शुद्धता प्राप्त की, जो BiLSTM मॉडल (86%) से अधिक थी। स्वतंत्र ब्लाइंड सेट पर परीक्षण के दौरान, SVM और BiLSTM ने क्रमशः 75% और 70.09% की शुद्धता हासिल की। विशेष रूप से, *Omicron*

सबवेरिएंट्स के वर्गीकरण में SVM मॉडल ने उल्लेखनीय 96% शुद्धता प्राप्त की। ये परिणाम दर्शाते हैं कि SERS को ML के साथ जोड़ने से वेरिएंट पहचान की संकल्प क्षमता और सटीकता में उल्लेखनीय वृद्धि होती है, जो वास्तविक समय महामारी विज्ञान निगरानी के लिए एक आशाजनक मार्ग प्रस्तुत करती है।

समानांतर रूप से, एंटीमाइक्रोबियल सस्पेंडिबिलिटी टेस्टिंग (AST) के महत्व को ध्यान में रखते हुए, हमने एक अभिनव बाइमेटलिक SERS सबस्ट्रेट विकसित किया, जिसमें गोल्ड नैनोआइलैंड्स को सिल्वर नैनोरोड्स (AuNI@AgNR) पर सजाया गया। यह GLAD और थर्मल डिपोजिशन तकनीक द्वारा निर्मित किया गया। गोल्ड नैनोआइलैंड्स की उपस्थिति ने न केवल सबस्ट्रेट की ऑक्सीकरण प्रतिरोधक स्थिरता बढ़ाई, बल्कि प्लाज़्मोनिक कपलिंग को भी महत्वपूर्ण रूप से उन्नत किया, जिससे विद्युतचुंबकीय क्षेत्र प्रवर्धन अधिक हुआ। AuNI@AgNR सबस्ट्रेट ने बैक्टीरियल रोगजनकों का अत्यंत निम्न सांद्रता (1 CFU/mL तक) पर, एकल और मिश्रित बैक्टीरियल कल्चर्स दोनों में, सफल पता लगाना संभव बनाया। इस प्लेटफॉर्म ने ग्राम-पॉज़िटिव और ग्राम-नेगेटिव बैक्टीरिया के बीच स्पष्ट अंतर किया तथा विभिन्न बैक्टीरियल स्ट्रेन्स के न्यूनतम अवरोधक सांद्रता (MICs) का शीघ्र निर्धारण किया। पार्टियल लीस्ट स्क्वैर डिस्क्रिमिनेंट एनालिसिस (PLS-DA) ने एंटीबायोटिक-संवेदनशील और रेज़िस्टेंट स्ट्रेन्स के बीच स्पष्ट वर्गीकरण को और भी सक्षम बनाया, जिससे AMR प्रोफ़ाइलिंग हेतु प्लेटफॉर्म की उपयोगिता सिद्ध होती है। विशेष रूप से, पॉलीमाइक्रोबियल संक्रमणों में बैक्टीरियल जनसंख्या को अलग करने और निगरानी करने की क्षमता वास्तविक परिस्थितियों में पॉइंट-ऑफ़-केयर (POC) अनुप्रयोगों की दिशा में एक महत्वपूर्ण प्रगति है।

अंततः, परजीवी संक्रमणों के बोझ को संबोधित करने हेतु, हमने मलेरिया की पहचान के लिए एक पोर्टेबल SERS प्लेटफॉर्म विकसित किया, जो हीमोज़ोइन के पैरामैग्नेटिक गुणों का उपयोग करता है — यह एक

अद्वितीय क्रिस्टलीय उपउत्पाद है जो केवल मलेरिया परजीवी द्वारा उत्पन्न होता है। GLAD द्वारा निर्मित AgNR सबस्ट्रेट्स का उपयोग करते हुए, रमन मापन के दौरान 0.3 T का बाहरी चुंबकीय क्षेत्र लगाया गया, जिससे SERS सिग्नल की तीव्रता में उल्लेखनीय दस गुना वृद्धि प्राप्त हुई, जो गैर-चुंबकीय परिस्थितियों की तुलना में थी। इस चुंबकीय सहायता ने अभूतपूर्व 10^{-14} M (लगभग 6 परजीवी/ μ L) की LOD संभव बनाई, जो पारंपरिक सीमाओं से कहीं अधिक है। क्रमिक डायल्यूशन अध्ययनों में प्रदर्शित किया गया कि हीमोग्लोबिन-संबंधित शिखरों के घटने के साथ हीमोज़ोइन संकेत SERS स्पेक्ट्रा में प्रमुख हो गए, जिससे चुंबकीय प्रभाव के तहत हीमोज़ोइन का विद्युतचुंबकीय हॉटस्पॉट्स पर प्राथमिक स्थानीयकरण सत्यापित हुआ। स्वस्थ और मलेरिया-पॉज़िटिव संपूर्ण रक्त और प्लाज़्मा नमूनों के SERS स्पेक्ट्रा पर प्रिंसिपल कंपोनेंट एनालिसिस (PCA) ने स्पष्ट क्लस्टरिंग दर्शाई, जिससे इस विधि की विश्वसनीयता और मज़बूती सिद्ध हुई। विशेष रूप से, चुंबकीय और गैर-चुंबकीय मलेरिया-पॉज़िटिव नमूनों ने PCA स्पेस में अलग-अलग क्षेत्र घेर लिए, जो पहचान की विश्वसनीयता पर चुंबकीय क्षेत्र प्रवर्धन के गहन प्रभाव को उजागर करता है।

संपूर्णतः, यह शोध प्रबंध उन्नत नैनोमैटेरियल्स, SERS तकनीकों और मशीन लर्निंग एल्गोरिद्म के एकीकरण की अपार संभावनाओं को प्रदर्शित करता है, जो बैक्टीरियल, वायरल और परजीवी रोगजनकों की पहचान हेतु शक्तिशाली, लचीले और संवेदनशील प्लेटफॉर्म स्थापित कर सकते हैं। विकसित रणनीतियाँ न केवल संवेदनशीलता और विशिष्टता की सीमाओं को आगे बढ़ाती हैं, बल्कि वास्तविक नैदानिक अनुप्रयोगों, महामारी निगरानी और एंटीमाइक्रोबियल प्रबंधन की दिशा में भी मार्ग प्रशस्त करती हैं। भविष्य में, इन प्लेटफॉर्म का पूर्ण रूप से एकीकृत पोर्टेबल उपकरणों में रूपांतरण, पहुँच, किफ़ायतीपन और संसाधन-सीमित परिस्थितियों में उपयोगिता को और सुदृढ़ करेगा।

TABLE OF CONTENTS

CERTIFICATE	I
ACKNOWLEDGEMENTS	II
ABSTRACT	VI
TABLE OF CONTENTS	XV
LIST OF FIGURES	XXI
LIST OF TABLES	XXVIII
ABBREVIATIONS	XXIX
Chapter 1 Introduction and Literature	1-31
1.1 Raman Scattering	2
1.2 Surface Enhanced Raman Spectroscopy	5
1.2.1 Chemical Enhancement Mechanism	7
1.2.2 Electromagnetic Mechanisms	9
1.3 SERS Substrates	12
1.3.1 Random morphology SERS Substrates	13
1.3.2 Periodic or Uniform SERS Substrates	14
1.4 Glancing Angle Deposition	16
1.4.1 Setup Configuration of GLAD	19
1.5 SERS Applications	21
1.5.1 SERS in Biosensing and Disease Diagnosis	22
1.6 Motivation	24
1.7 Objectives of the Thesis	27
1.8 Thesis Overview	28

Chapter 2 Experimental and Characterization Technique	32-54
2.1 Growth Techniques	33
2.1.1 GLAD	33
2.1.2 Thermal Evaporation Technique	36
2.2 Substrate Packaging Unit	38
2.3 Characterization Techniques	40
2.3.1 X-Ray Diffraction Technique	40
2.3.2 Raman Spectroscopy	42
2.3.3 Atomic Force Microscopy	44
2.3.4 UV-Vis Spectroscopy	46
2.3.5 Electron Microscopy	49
2.3.5.1 FESEM	49
2.3.5.2 TEM	51
2.3.6 Contact Angle Measurements	53
Chapter 3 Paper Based SERS Substrates Fabricated by GLAD for Nosocomial Infection Detection	55-88
3.1 Introduction	56
3.2 Experimental Section	62
3.2.1 Development of SERS Substrates	62
3.2.2 Bacteria Culture	63
3.2.3 SERS Measurements	64
3.3 Results and Discussion	66
3.3.1 SERS Substrate Characterization	66

3.3.2 Adsorption and Hydrophobicity	70
3.3.3 Paper Substrate in Detecting PA from Mixture of PBS Salts	72
3.3.4 Impact of SERS Platform on Bacterial Load	87
3.3.5 Gram Positive and Negative Bacteria Detection	80
3.3.6 Peak Assignments	81
3.4 Conclusion	87
Chapter 4 SERS Detection of SARS CoV2 Variants and Subvariants from NPS Swabs using Ag Nanorods with Machine Learning	89-131
4.1 Introduction	90
4.2 Experimental	96
4.2.1 Synthesis of Ag NR Substrates	96
4.2.2 Isolation of SARS CoV2 Variants and Clinical NPS Samples	97
4.2.3 SERS Measurements	98
4.2.4 Data Processing and ML Model Training	98
4.3 Results and Discussion	102
4.3.1 Characterization of Ag NR Substrates	102
4.3.2 Performance of Ag NR Substrates	105
4.3.3 SERS Detection of SARS CoV2 Samples	107
4.3.4 Detection of Different Sub-Variants of Omicron	115
4.3.5 Clinical Validation of SERS Platform using ML SERS	120
4.4 Conclusion	130
Chapter 5 GLAD Fabricated Gold Capped Ag Nanorods as SERS Substrates for Polymicrobial Detection and Antibiotic Susceptibility Testing	132-185

5.1 Introduction	133
5.2 Experimental	138
5.2.1 Materials	138
5.2.2 Fabrication of Substrates	139
5.2.3 Characterizations	139
5.2.4 Bacteria Culture	140
5.2.5 SERS Measurements	141
5.2.6 FDTD Simulations	141
5.2.4 Statistical Analysis	142
5.3 Results and Discussion	143
5.3.1 Characterization of Au NI@Ag NR	143
5.3.1.1 Morphological Elucidations	143
5.3.1.2 Structural and Compositional Analysis	147
5.3.2 FDTD Simulation Results	151
5.3.3 SERS Measurements on Au NI@Ag NR	152
5.3.3.1 SERS Spectra of BPE Molecule	152
5.3.3.2 Reproducibility and Stability Studies	153
5.3.3.3 SERS Detection of Four Different Bacteria	157
5.3.3.4 SERS of bacteria spiked in serum	162
5.3.3.5 Detection of Antibiotic resistance E.coli	164
5.3.3.6 Multiplex SERS Detection of Mix Bacteria	167
5.3.3.7 SERS-based Monitoring of Amoxicillin on E.coli	170

5.3.3.8 Mix Bacteria Treated with Amoxicillin	174
5.3.3.9 Mix Bacteria Treated with Imipenem	177
5.3.3.10 PLS-DA Analysis	181
5.4 Conclusion	183
Chapter 6 Hand-held Portable SERS Platform for Detection of Malarial Parasites Using External Magnetic Field	186-210
6.1 Introduction	187
6.2 Experimental	192
6.2.1 Fabrication of SERS Substrates	192
6.2.2 Characterization of SERS Substrates	193
6.2.3 Collection of Blood and Plasma Samples	193
6.2.4 SERS Measurements	194
6.2.5 Statistical Analysis	194
6.3 Results and Discussion	195
6.3.1 Characterization of Ag NR Arrays	195
6.3.2 SERS Detection of Malaria from Whole Blood	198
6.3.3 SERS Studies in Presence and Absence External Magnetic Field	201
6.3.4 Detection of Malaria from Plasma Samples	206
6.3.5 Multivariate Analysis using PCA	208
6.4 Conclusion	210
Chapter 7 Conclusion and Future Prospectives	211-215
7.1 Summary and Conclusions	212
7.2 Scope for Future Work	214

References	216
Publications	245
Biodata	249

LIST OF FIGURES

Figure 1.1. Energy level diagram representing the phenomenon of Rayleigh and Raman scattering.....	3
Figure 1.2. SERS mechanism for detection of analyte molecule.....	6
Figure 1.3. Localized surface plasmon resonance.....	9
Figure 1.4. Schematic diagram showing glancing angle deposition (GLAD) experimental setup.....	20
Figure 1.5. Current techniques used in disease diagnosis and how SERS merits can be the new paradigm in the field of diagnosis.....	23
Figure 2.1. (a) Schematic showing working of GLAD technique (b) Digital photograph of homemade customized GLAD setup with fixed substrate angle.....	36
Figure 2.2. Schematic diagram for thermal evaporation setup.....	37
Figure 2.3. (a) Substrate packaging unit with N ₂ gas filling and lamination capability. (b) Packed SERS substrates of Ag nanorods in an Aluminum packet filled with inert N ₂ gas.....	39
Figure 2.4. Schematic diagram of XRD setup.....	41
Figure 2.5. Schematic diagram of a typical Raman spectrometer showing main components.....	43
Figure 2.6. Raman spectrometer used for Raman and SERS studies: (a) Renishaw inVia Raman microscope; (b) Hand-held Raman spectrometer made of AssurX.....	44
Figure 2.7: Schematic diagram of the atomic force microscopy.....	46
Figure 2.8. Schematic representation of UV-ViS setup.....	48
Figure 2.9 (a) Schematic diagram showing FESEM principle (b) Image of the FESEM TESCAN.....	51
Figure 2.10. Schematic diagram showing main components of transmission electron.....	52
Figure 2.11. Image of the Kruss DSA25E drop shape analyzer.....	54

Figure 3. 1. An illustration of the innovative paper-based novel substrate for SERS dependent bacterial detection.....	61
--	----

Figure 3.2. FESEM images of (a) plain paper without any deposition. (b) AgNR deposited on paper substrate using GLAD. High-resolution picture of zigzag 2-arm AgNR produced on (c) paper substrate; (d) glass substrate.....	68
--	----

Figure 3.3. FESEM image of zigzag AgNR grown on paper substrate, (b-d) EDX elemental maps of the zigzag AgNR paper substrate depicting the uniform deposition of Ag in the zigzag morphology (e) EDX spectrum of paper based zigzag AgNR substrate showing pristine substrate. (f) XRD spectrum of zigzag AgNR paper-based substrate. (g) UV-vis reflectance spectra of both, AgNR zigzag structure grown on glass and paper substrates.....	69
--	----

Figure 3.4. Contact angle measurements (a) immediately after water was drop-casted on the 2-arm AgNR grown paper substrate, and (b) after 32 mins. Contact angle for AgNR deposited on glass substrate at time=0 min (b) Contact angle for AgNR deposited on glass substrate at time=16 min.....	71
--	----

Figure 3.5. SERS spectra of different concentrations of <i>P. aeruginosa</i> on (a) zigzag AgNR glass substrate and (b) on zigzag AgNR paper substrate.....	74
---	----

Figure 3.6. Comparison of the intensity of SERS spectra for <i>P. aeruginosa</i> in (a) neat, (b) 1:1 and (c) 1:10 diluted bacterial suspension on the zigzag paper based AgNR and glass based AgNR substrates.....	75
---	----

Figure 3.7. (a) SERS intensity profile for <i>P. aeruginosa</i> from 10 different spots on zigzag AgNR paper substrate; (b) Variation of 647 and 721 cm^{-1} peak intensity from 10 different locations paper-based SERS substrate.....	76
--	----

Figure 3.8. SERS spectra for <i>S. aureus</i> for the range varying between 102 cp/mL to 108 cp/mL drop-casted on (a) zigzag AgNRs on paper substrates and (b) zigzag AgNRs on glass substrates.....	77
--	----

Figure 3.9. A comparison of the intensity of the SERS spectra for <i>S. aureus</i> on the AgNR grown on paper substrate and glass substrate for the concentrations ranging between 102 cp/mL to 108 cp/mL [(a) 108 cp/mL (b) 106 cp/mL (c) 104 cp/mL (d) 102 cp/mL.....	79
---	----

Figure 3.10. SERS spectra of <i>S. aureus</i> (gram +ve strain), <i>E. coli</i> (gram -ve strain) and <i>P. aeruginosa</i> (gram -ve strain) detected on (a) 2-arm AgNR on paper substrate (b) 2-arm AgNR on glass substrate.....	81
---	----

Figure 3. 11. (a) FESEM image of bacteria *S. aureus* adsorbed on zigzag AgNR paper substrate (b-d) EDX elemental maps of the zigzag AgNR paper substrate with bacteria adsorbed on it depicting the integrity of the interacting bacteria with SERS substrate.....86

Scheme 4.1. Process of detection of the SARS-CoV-2 variants using ML-integrated SERS platform.....95

Figure 4.1. (a) FESEM showing the uniform distribution of Ag nanorods; (b) EDX analysis revealing the presence of highly pure AgNRs on the Ti layer (c) TEM image showing the length and width of a single nanorod; (d) 2D AFM images of the surface of the AgNR arrays as synthesized, respectively, for the scan size 5x5 μ m.....102

Figure 4.2. (a) EDX spectrum highlighting the Ag peak, indicates high purity of the nanorods with no discernible impurities. (b) XRD patterns confirming the crystalline structure of the AgNRs. (c) UV-vis absorbance spectra of the AgNRs, with peaks at 452 nm and 501 nm (d) Contact angle of 32.5° on Ti thin film surface (e) Contact angle of 105° after deposition of silver nanorods....104

Figure 4.3. (a) Comparison of BPE SERS spectra at different concentrations with those obtained from a standard Ag thin film (b) Relationship between the intensity of the 1644 cm⁻¹ peak and the concentration of BPE, showing a consistent correlation with an R² value of 0.97.....106

Figure 4.4. SERS spectra for dilutions (100 times and 1000 times) for (a) Wildtype (b) Kappa (c) Delta (d) BA.1 (e) BA.2 (f) BA.5 (g) XBB strains of SARS-CoV2. The viruses were quantified using plaque assay which was further diluted with NFW to determine the sensitivity of the SERS platform.....109

Figure 4.5. Plot showing SERS spectra of all the strains and sub-strains of SARS-CoV2 virus isolated and cultured in VERO cells where (a) wildtype (b) XBB (c) BA.5 (d) BA.1 (e) BA.5 (f) Kappa (g) Delta. The strains were isolated from the COVID-19 positive patients confirmed with q-RT-PCR and NGS. The virus stocks were quantitated using a plaque assay.....110

Figure 4.6. (a) Illustrates the average SERS spectra of four different strains of SARS-CoV2 isolates (WT, Kappa, Delta, Omicron) and uninfected Vero cells. The highlights in cyan shows the peaks conserved in all the 4 strains (b) shows the comparison of spectra between Delta and Kappa strain. The highlights in blue marks the difference in peak between the 2 strains (c) shows the spectral comparison between Delta and Omicron strain. The highlight in orange marks the differences between the strains.....112

Figure 4.7. (a) SERS measurements from 5 different spots of Kappa strain where RSD was determined for 733 and 1436 cm^{-1} (b) SERS measurements from 5 different spots of Omicron strain (BA.1 sub-strain) where RSD was determined for 733 and 1338 cm^{-1} depicting the uniformity of the signals... 115

Figure 4.8. (a) Illustrates spectra of four sub strains of the Omicron strain with common peaks between the sub-strains highlighted in green (b) Comparison between BA.1 and BA.5 sub strains, almost similar pattern between the two sub-strains (c) Comparison between BA.2 and XBB sub strains of omicron, with 1049 cm^{-1} peak unique to XBB only marked in pink..... 116

Figure 4.9. 920 cm^{-1} peak highlighted and shown in all the sub-strains of Omicron variant..... 119

Figure 4.10: Average SERS spectra of NPS collected from patients of negative and positive COVID-19 with blue highlights showing the distinguishing peaks between negative NPS and positive NPS samples..... 121

Figure 4.11: PCA plot showing distribution of samples; (a) PCA plot showing distribution of SARS-CoV-2 variants and (b) PCA plot showing distribution of SARS-CoV-2 Omicron sub-variants..... 125

Figure 4.12: Performance of classification model on validation set; (a) Table showing accuracy, precision, recall and f1-score for SVM and BiLSTM models; (b) and (c) Confusion matrix for SVM and BiLSTM models..... 126

Figure 4.13. Performance of classification model on blind samples testing set; (a) Table showing accuracy, precision, recall and f1-score for SVM and BiLSTM model; (b) and (c) Confusion matrix for SVM and BiLSTM model..... 127

Figure 4.14. Performance of classification model (Omicron sub-variant classifier) on validation set; (a) Table showing accuracy, precision, recall and f1-score and (b) Confusion matrix for Omicron sub-variant classifier (SVM model)..... 128

Figure 4.15: SHAP summary plot showing contribution of top 20 features in SVM model prediction; (a) SHAP summary plot for SARS-CoV-2 variant classification model (SVM) and (b) SHAP summary plot for Omicron sub-variant classification model (SVM)..... 129

Scheme 5.1. A highly sensitive and stable SERS substrate using AuNI@AgNR for detection of multiple bacteria and antibiotic susceptibility testing..... 138

Figure 5.1. FESEM and EDX of AuNI@AgNR substrates (a) FESEM image showing uniformly distributed substrate (b-e) EDX mapping showing clear distribution of Au nanoislands on Ag nanorods (f) Elemental analysis shows pristine substrates without presence of any impurities..... 144

Figure 5.2. HR-TEM imaging of AuNI@AgNR substrates. (a-c) Shows the morphology and SAED pattern of Ag nanorods (d) shows the morphology of Ag nanorods with Au nanoislands, with length of a single rod to be around 900nm (e) size of nanoislands are found to be around 30nm (f) D-spacing and SAED pattern of Au nanoislands.....145

Figure 5.3. AFM imaging of AuNI@AgNR (a) Ag nanorods (b) Au-decorated AgNR with 30nm Au deposited (c) Au-decorated AgNR with 80nm Au decorated (d) table showing the substrates with the respective roughness.....146

Figure 5.4. AuNI@AgNR characterizations: (a) XRD spectra for both AgNR and AuNI@AgNR substrates (b) UV-Vis spectra showing both absorbance and reflectance of substrates (c) XPS survey spectra for AgNR and AuNI@AgNR substrates (d) XPS spectra of Ag 3d and Au 4f.....147

Figure 5.5. Contact angle measurements on AuNI@AgNR (a) Water droplet on bare AgNR (b) Water droplet on bare AuNI@AgNR (c) E. coli drop casted on AuNI@AgNR substrate (d) S. aureus drop casted on AuNI@AgNR.....149

Figure 5.6. FDTD simulation results depicting the electromagnetic field distribution for (a) top view and (b) side view of AgNRs, and (c) top view and (d) side view of gold-coated AgNRs.....151

Figure 5.7. (a) Enhanced SERS spectra of BPE molecules on AuNI@AgNR substrate. (b) Linear fit curve showing adj. R2 value 0.99. Intensity map for prominent peaks of BPE (c) 1612 cm⁻¹; (d) 1012 cm⁻¹; over 5×5 μm area. (e) Intensity profile of SERS spectra measured from 26 random locations on AuNI@AgNR substrate. (d) Variation of intensity over random spots for calculating RSD.....155

Figure 5.8.(a) SERS spectra of E. coli bacteria measured over different days on AuNI@AgNR substrate for stability studies. (b) SERS spectra measured over different days on AgNR substrate for stability studies. (c) The intensity variation of dominant peak of E. coli for 28 days over an interval of every 3 days.....156

Figure 5.9. SERS spectra of 4 different bacteria captured on AuNI@AgNR substrate (a) E. coli bacteria (b)P. aeruginosa bacteria (Gram-negative) (c) and (d) FESEM image of E. coli and P. aeruginosa bacteria on AuNI@AgNR substrates (e) SERS spectra of S. aureus bacteria; (f) B. subtilis bacteria (Gram-positive bacteria) (g) and (h) FESEM image of S. aureus and B. subtilis bacteria drop casted on AuNI@AgNR substrates.....159

Figure 5.10. SERS spectra collected on AuNI@AgNR of bacteria spiked serum and control serum	163
Figure 5.11. SERS spectra collected on AuNI@AgNR for (a) E. coli and its resistant strains (b) Different ratios of mix culture of S. aureus and E. coli bacteria (c) Different ratios of mix culture of four bacteria (i.e. 2 gram positive and 2 gram negative).....	166
Figure 5.12. Effect of different concentrations of Amoxicillin on E.coli (a) Raman spectra of E.coli after treating with 0.1mg/mL of antibiotics at different time points (1 hr, 3 hrs and 20 hrs) (b) Raman spectra of E.coli after treating with 0.5 mg/mL of antibiotics on E.coli at different time points (c) Raman spectra of E.coli after treating with 1 mg/mL of antibiotics on E.coli at different time points (d) SERS spectra of E.coli after treating with 2 mg/mL, 5 mg/mL and 10 mg/mL of antibiotics after 1 hr of incubation.....	171
Figure 5.13. FESEM images of S. aureus after treating with different conc. of antibiotics (a-b) 0.1 mg/mL of Amoxicillin (c-d) 0.5 mg/mL (e-f) 2 mg/mL of (g-h) 5 mg/mL of amoxicillin.....	173
Figure 5.14. Different concentrations of Amoxicillin (0.01, 0.1, 0.5, 1, 2, 5 and 10 mg/mL) with different ratios of Gram-positive and Gram-negative bacteria (a) 1:1 ratio (b) 2:1 ratio (c) 1:2 ratio.....	175
Figure 5.15. Line plots representing normalized SERS peak intensities at different concentrations of Amoxicillin for each bacterial ratio (a) 1:1 ratio (b) 2:1 ratio (c) 1:2 ratio.....	176
Figure 5.16. Different concentration of Imipenem (0.1, 0.5, 1, 2, 5 and 10 mg/mL) with different ratios of mix bacteria (a) 1:1 ratio of Gram-positive to Gram-negative bacteria (b) 2:1 ratio of Gram-positive to Gram-negative bacteria (c) 1:22 ratio of Gram-positive to Gram-negative bacteria (d, e, f) Heatmap analysis providing a comprehensive visualization of spectral variations in bacterial mixtures treated with imipenem.....	179
Figure 5.17. PLS-DA of bacteria: (a) Clear distinction between susceptible and resistant E. coli types (b) Distinction between four different bacteria belonging to Gram positive and negative groups (c) Mix culture of 2 Gram positive and Gram-negative bacteria in 1:1, 2:1 and 1:2 ratio.....	182
Scheme 6.1. The malaria infection from a bite to the compromise of RBCs...	189
Scheme 6.2. Schematic diagram showing detection of malaria using AgNR substrates with an external magnetic field for SERS detection from whole blood samples.....	191

Figure 6.1. (a) FESEM imaging showing the high uniformity distribution of silver nanorods on substrates (b) The diameter of nanorods was found to around 80nm (c) Purity of the substrates using EDX mapping showing pure Ag distribution (d) Traces of oxygen in the substrate (e) UV-VIS showing high absorption of the AgNR substrates (f). Shows XRD data implying the dominance of FCC phase.....196

Figure 6.2. (a) SERS spectra of μM MB over AgNRs array (b) Raman spectra of 1 M MB over conventional Ag film.....197

Figure 6.3. SERS spectra of whole blood malaria-positive and healthy samples drop-casted directly on label-free AgNR substrate.....199

Figure 6. 4. SERS spectra for different dilutions of patient blood, where the data has been collected (a) without application of the magnetic field and (b) with the application of a magnetic field.....203

Figure 6.5. SERS spectra of malaria positive blood samples with and without external magnetic field (a) for 10^{-6}M (b) for 10^{-9}M (c) for 10^{-12}M (d) 10^{-14}M204

Figure 6. 6. Spectral range from 800 to 1500 cm^{-1} for increasing in dilution of the blood sample.....205

Figure 6.7. (a) 1:50 and 1:20 dilution of healthy plasma (b) 1:50 and 1:20 dilutions of malaria positive plasma (c) 1:20 dilution of patients' and healthy plasma (d) 1:50 dilution of patients' and healthy plasma.....207

Figure 6.8. PCA scatter plot for clinical samples (a) blood samples (b) plasma samples.....209

LIST OF TABLES

Table 3.1: Raman peaks that played significance in bacteria and description of biochemical alterations occurring among species.....	83
Table 3.2: Comparison of GLAD method of fabrication of nanostructures on paper with other commonly used methods.....	86
Table 4.1: Distribution of NPS samples with their corresponding spectral data for the four variants of SARS-CoV-2.....	101
Table 4.2: Comparison and peak assignment of the four SARS-CoV2strains.....	113
Table 4.3: RSD of prominent peaks of kappa and omicron variants.....	114
Table 4.4: Peak assignment of Raman spectra of Omicron sub-variants. Green highlighted peaks are found to be conserved across all the sub-variants.....	117
Table 4.5: Comparison of other respiratory viruses (Adenovirus, Rhinovirus, RSV and Influenza virus) with COVID-19 positive and negative clinical NPS.....	124
Table 4.6: Shows the clear output of both the models on training, testing and validation sets for NPS patient samples for strains and omicron virus sub-variants.....	130
Table 5.1: BPE peaks with their corresponding RSD %.....	154
Table 5.2: Signal retention from both substrates observed over 28 days...	157
Table 5.3. Raman peak assignment for Gram-negative bacteria.....	161
Table 5.4. Raman peak assignment for Gram-positive bacteria.....	162
Table 6.1: shows the clear peak assignment of healthy and malaria-positive samples with their corresponding dominating peaks highlighted.....	201
Table 6.2: shows the enhancement fold for each dilution with and without an external magnetic field.....	205
Table 6. 3: Peak assignment for blood plasma.....	208

ABBREVIATIONS

SERS	Surface Enhanced Raman Spectroscopy
AMR	Antimicrobial Resistance
MIC	Minimum Inhibitory Concentration
AST	Antibiotic Susceptibility Test
NGS	Next Generation Sequencing
PCR	Polymerase Chain Reaction
DNA	Deoxyribonucleic Acid
RNA	Ribonucleic Acid
RS	Respiratory Viruses
ELISA	Enzyme Linked Immunosorbent Assay
DOS	Density of states
EM	Electromagnetic enhancement
CE	Chemical enhancement
vdW	van der Waals
XRD	X-ray diffraction
FESEM	Field electron scanning electron microscopy
GLAD	Glancing angle deposition
OAD	Oblique angle deposition
XPS	X-ray photoelectron spectroscopy
SPR	Surface plasmon resonance
B.E.	Binding energy
PVD	Physical vapor deposition
3D	Three dimensional
EDX	Electron diffraction analysis
EPMA	Electron Probe Microanalyzer
TEM	Transmission electron microscopy

HRTEM	High-resolution transmission electron microscopy
AFM	Atomic force microscopy
TMDC	Transition metal dichalcogenides
PECVD	plasma-enhanced chemical vapor deposition
SERS	Surface enhanced Raman spectroscopy
OC	Oral cancer
ML	Machine Learning
JCPDS	Joint Committee on Powder Diffraction Standards
MO	Methyl orange
MB	Methylene blue
BPE	trans-1,2-bis(4-pyridyl)ethylene
EC	E. Coli
SA	S. Aureus
RhB	Rhodamine B
BSE	Backscattered electron
CFU	Colony Forming Unit
PVD	Physical vapor deposition
PVA	Polyvinyl alcohol
EDS	Energy dispersive spectrometer
CB	Conduction band
VB	Valance band
SP	Surface potential
KPFM	Kelvin probe force microscopy
CCD	Charge coupled device
LOD	Limit of detection
PBS	Phosphate Buffered Saline